

Complex phase separation in $\text{La}_{0.6}\text{Ca}_{0.4}\text{MnO}_3$ films revealed by electron spin resonance

A. I. Tovstolytkin, V. V. Dzyublyuk, and D. I. Podyalovskii
Institute of Magnetism, 36b Vernadsky Boulevard, Kyiv 03142, Ukraine

X. Moya, C. Israel, D. Sánchez, M. E. Vickers, and N. D. Mathur
Department of Materials Science, University of Cambridge, Cambridge, CB2 3QZ, United Kingdom
 (Received 14 July 2010; revised manuscript received 8 February 2011; published 16 May 2011)

We have used electron spin resonance to study an epitaxial thin-film sample of the manganite $\text{La}_{0.6}\text{Ca}_{0.4}\text{MnO}_3$ in which ferromagnetic and paramagnetic phases were previously shown to coexist [Phys. Rev. B **78**, 054409 (2008)]. Resonant absorptions arise on either side of the paramagnetic resonance and reveal that the ferromagnetic phase is itself phase separated into regions with Curie temperatures of ~ 190 and ~ 250 K. This extra complexity is attributed to the coexistence of strained and relaxed regions, as verified by x-ray diffraction.

DOI: [10.1103/PhysRevB.83.184404](https://doi.org/10.1103/PhysRevB.83.184404)

PACS number(s): 75.47.Lx, 75.70.-i

I. INTRODUCTION

Doped perovskite manganites such as $\text{La}_{1-x}\text{AE}_x\text{MnO}_{3\pm\delta}$ (alkaline earth $\text{AE} = \text{Ca, Sr, Ba}$) have attracted much attention during the past two decades, sparked by the discovery of colossal magnetoresistance (CMR) around the Curie temperature T_C .^{1,2} Near or just below room temperature, the manganites develop magnetically and/or electronically ordered phases as a result of competition between highly spin-polarized ferromagnetic (FM) metallic phases and charge-ordered (CO) insulating phases. The FM phases arise when mobile electrons couple Mn core spins via double exchange.³ The CO phases have traditionally been associated with Jahn-Teller distortions of Mn ions that were each assumed to trap an entire valence electron, but overinterpretation has led to controversy.⁴

The competing physics in doped manganites causes traditional and also peculiar phases to arise⁵⁻⁷ and coexist^{5,7,8} over a wide range of length scales. The balance between competing phases may be tuned via small changes in either intrinsic parameters such as doping, or extrinsic parameters such as magnetic field and temperature.^{9,10} Strain plays a particularly significant role^{11,12} and therefore sample morphology can strongly influence physical properties. Epitaxial films on which we focus here are desirable for studying basic manganite physics in the absence of extrinsic effects associated with grain boundaries and twin boundaries.

Magnetic and electronic phase separation is commonly observed in many manganites. It has attracted widespread interest over the past decade¹³ and may be exploited to yield memory effects associated with local variations in FM phase fraction,^{14,15} cf. phase-change random access memory (PC-RAM). We recently exploited phase separation in epitaxial thin-film $\text{La}_{0.6}\text{Ca}_{0.4}\text{MnO}_3$ in order to magnetically decouple FM manganite electrodes of $\text{La}_{0.7}\text{Ca}_{0.3}\text{MnO}_3$ and thus demonstrate two-state low-field magnetoresistance effects in trilayer structures grown on NdGaO_3 (001) substrates.¹⁶

Although bulk $\text{La}_{0.6}\text{Ca}_{0.4}\text{MnO}_3$ lies well within the FM phase field and has a FM volume fraction approaching 100%,¹⁷ epitaxial films of $\text{La}_{0.6}\text{Ca}_{0.4}\text{MnO}_3$ grown by pulsed laser deposition on NdGaO_3 (001) substrates possess a $\sim 50\%$ FM volume fraction that coexists with a $\sim 50\%$ paramagnetic

(PM) insulating phase.¹⁸ In Ref. 16 we investigated the microscopic nature of this phase separation in a 55-nm film of this type, which as expected¹⁸ had a Curie temperature of ~ 150 K, a low-temperature FM volume fraction of $\sim 42\%$, and a metal-insulator transition temperature at ~ 145 K. Using conducting-tip atomic force microscopy (CTAFM) and magnetic force microscopy (MFM), we concluded that our 55-nm film contains FM metallic regions within a PM matrix. We further concluded that some of these FM regions are isolated, but that most form a three-dimensional network of filamentary conducting pathways. This network was found to be invariant across cooling runs, suggesting that it is created by frozen-in local strain fields.

Here we use electron spin resonance (ESR) as an alternative microscopic probe of exactly the same 55-nm film of $\text{La}_{0.6}\text{Ca}_{0.4}\text{MnO}_3$ on NdGaO_3 that was characterized and then studied using CTAFM and MFM in Ref. 16. ESR has been used previously to successfully show phase separation in 200-nm-thick films of $\text{La}_{0.5}\text{Ca}_{0.5}\text{MnO}_3$ on LaAlO_3 and MgO substrates,¹⁹ and we find that ESR distinguishes the FM and PM phases as expected.²⁰ Surprisingly, we also find that the FM regions are themselves phase separated into regions that we identify to be strained and relaxed. Results from x-ray diffraction support this assignment.

II. EXPERIMENTAL

X-ray diffraction (XRD) data were collected using a high-resolution Panalytical diffractometer with a four-bounce primary monochromator and a three-bounce analyzer crystal. Absolute values of film lattice parameters were established from (116) $\text{La}_{0.6}\text{Ca}_{0.4}\text{MnO}_3$ film reflections measured relative to the (116) NdGaO_3 substrate reflection, for which the orthorhombic lattice parameters are known with precision to be $a = 5.4276$ Å, $b = 5.4979$ Å, and $c = 7.7078$ Å.²¹ In principle, reflections such as (316) and (136) would enable a and b to be determined independently, but these reflections are too weak for the satellite reflections of interest to be observed (A and B in Fig. 1), and so, in practice, we have assumed the NdGaO_3 unit cell to be tetragonal ($a = b = 3.8628$ Å and $c = 3.8539$ Å).

The ESR studies were carried out in 110–270 K using an x-band ELEXSYS E500 EPR spectrometer (Bruker BioSpin GmbH, Germany). The measurements were performed at $\nu = 9.44$ GHz with applied magnetic field \mathbf{H} either parallel or perpendicular to the film plane. Three parameters can be extracted from ESR spectra: intensity I , which provides information about the relative FM and PM phase fractions; resonance field H_0 , from which the magnetization of ferromagnetic species can be calculated; and peak-to-peak linewidth ΔH , which is extracted from dI/dH vs H , and indicates the degree of inhomogeneity in the local magnetization.

For a bulk manganite in the PM phase above T_C , the resonance signal is a symmetric line centered at

$$H_0^{\text{PM}} = \omega/\gamma, \quad (1)$$

where ω is angular frequency, γ is the gyromagnetic ratio ($\gamma = 2\pi g_{\text{eff}}\mu_B/h$),²² h is Planck's constant, μ_B is the Bohr magneton, and g_{eff} is the effective g factor which for doped manganites is usually close to the free-electron value of 2.0023 or only slightly different.^{23–26} The value of H_0^{PM} displays a negligible dependence on temperature and magnetic-field direction.^{23,24} On lowering the temperature, I grows monotonically but ΔH exhibits nonmonotonic changes with a minimum slightly above T_C .^{27–29}

Below T_C , magnetic resonance in the FM state is governed by the effective magnetization, and this depends on the spontaneous magnetization M_0 as well as anisotropies due to shape, strain, and crystallinity.^{22,30} For thin films, in which we assume anisotropy only due to shape, the resonances in homogeneous regions may be described using the Kittel formulas with appropriate demagnetizing factors:

$$(\omega/\gamma)^2 = H_0^{\parallel}(H_0^{\parallel} + 4\pi M_0), \quad (2)$$

$$\omega/\gamma = H_0^{\perp} - 4\pi M_0, \quad (3)$$

where H_0^{\parallel} and H_0^{\perp} are, respectively, the resonance fields for \mathbf{H} parallel and perpendicular to the film plane in which the magnetization lies.³⁰ Equations (1)–(3) imply $H_0^{\parallel} < H_0^{\text{PM}}$ and $H_0^{\perp} > H_0^{\text{PM}}$, and the imbalances in these inequalities increase with decreasing temperature due to an increase in M_0 .

III. RESULTS AND DISCUSSION

Figure 1 shows a high-resolution XRD (116) reciprocal space map. The majority of the $\text{La}_{0.6}\text{Ca}_{0.4}\text{MnO}_3$ film is coherently strained as expected, and has in-plane lattice parameters $a = b \sim 3.862$ Å and an out-of-plane lattice parameter $c \sim 3.864$ Å using pseudocubic notation. The two satellites A and B, showing a weak and broad intensity near the main film reflection, are attributed to the relaxed regions of the film. For satellite A the relaxation increases the in-plane lattice parameter to ~ 3.865 Å and decreases the out-of-plane lattice parameter to ~ 3.861 Å, whereas for satellite B the relaxation decreases the in-plane lattice parameter to ~ 3.856 Å and increases the out-of-plane lattice parameter to ~ 3.869 Å. All three regions of the film have similar unit-cell volumes ($\sim 57.6 \pm 0.1$ Å³) that are slightly larger ($\sim 0.8\%$) than the unit-cell volume of the $\text{La}_{0.6}\text{Ca}_{0.4}\text{MnO}_3$ target as determined

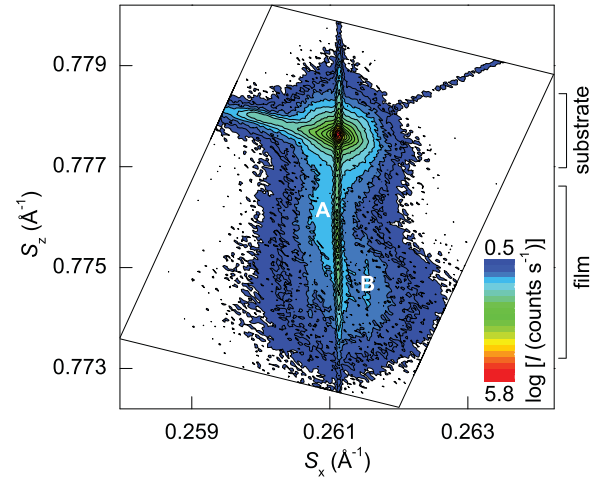


FIG. 1. (Color online) High-resolution XRD reciprocal space map of the $\text{La}_{0.6}\text{Ca}_{0.4}\text{MnO}_3$ film showing (116) reflections, where reciprocal lattice units S_x and S_z correspond to inverse lattice spacings. The NdGaO_3 substrate peak has the highest intensity I . The weaker peak with $S_x = 0.2611$ Å⁻¹ and $S_z = 0.7755$ Å⁻¹ comes from fully strained $\text{La}_{0.6}\text{Ca}_{0.4}\text{MnO}_3$ and the out-of-plane lattice parameter is similar to results from a high-resolution XRD ω - 2θ scan of the $\text{La}_{0.6}\text{Ca}_{0.4}\text{MnO}_3$ (004) symmetric reflection, where the out-of-plane lattice parameter $c \sim 7.729(2)$ Å (not shown). The vertical spread in the $\text{La}_{0.6}\text{Ca}_{0.4}\text{MnO}_3$ (116) reflection suggests a film thickness of ~ 60 nm that is consistent with the 55-nm thickness deduced in Ref. 16. Weak satellite intensities A and B may be seen near the $\text{La}_{0.6}\text{Ca}_{0.4}\text{MnO}_3$ (116) reflection. Two diagonal streaks, and a single vertical streak, arise near the NdGaO_3 reflection as a consequence of instrumental effects (Ref. 31).

via Rietveld analysis ($a = b = 3.8545$ Å and $c = 3.8463$ Å such that $a^2c = 57.144$ Å³). This volumetric discrepancy, which one of the authors (Vickers) has also observed for thin films of other materials systems, makes it impossible to say whether the observed relaxation is partial or complete. Varying degrees of structural relaxation could explain the spread of intensity near A and B, but so could finite-size effects and the orthorhombicity of NdGaO_3 , which is here assumed to be tetragonal.

Figure 2 shows the temperature evolution of the differential absorption curves dI/dH vs H , with \mathbf{H} applied parallel to the film plane. At 270 K, there is one broad line ($\Delta H \approx 980$ Oe) and one narrow line (line 1, $\Delta H \approx 16$ Oe). The former is the resonance signal from the PM phase^{24,25,32} with $g_{\text{eff}} \approx 2.025$, and it can be seen that I and ΔH depend strongly on temperature, as expected.^{28,29} Line 1 has parameters that show a negligible temperature dependence, suggesting that it does not arise from the film whose properties are strongly temperature dependent at least near T_C . If pure, the substrate cannot be responsible for line 1 either, as NdGaO_3 yields a negligible ESR signal.³³ However, paramagnetic impurities in NdGaO_3 are known to yield narrow ESR lines with little temperature dependence,^{24,34} and so we suggest that these are responsible for line 1.

At 170 K and below, the distinct signature of ferromagnetic resonance is seen at $H_0^{\parallel\text{FM}_s} < H_0^{\text{PM}}$ (dashed circle and arrow, Fig. 2), consistent with Eq. (2) for an in-plane magnetization of magnitude $M_0^{\text{FM}_s}$. Given such a low onset temperature

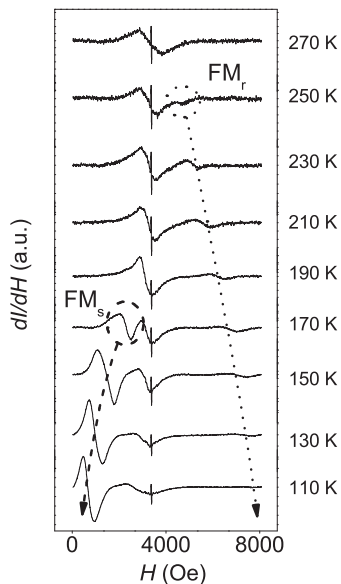


FIG. 2. Differential absorption dI/dH vs H at different temperatures measured on cooling, for \mathbf{H} applied parallel to the film plane. The narrow line (line 1) slightly below 4000 Oe is essentially temperature independent. The apparent variation in its height arises because the vertical scale varies between traces. Onsets for the resonances due to strained (s) and relaxed (r) FM regions are indicated.

relative to bulk FM manganites where $T_C \sim 250$ K,¹⁷ we suggest that this resonance comes from FM regions lying within the coherently strained part of the film, and we denote this strained (s) phase FM_s . Later (Figs. 3 and 4) we show that this resonance persists to 190 K rather than 170 K, and

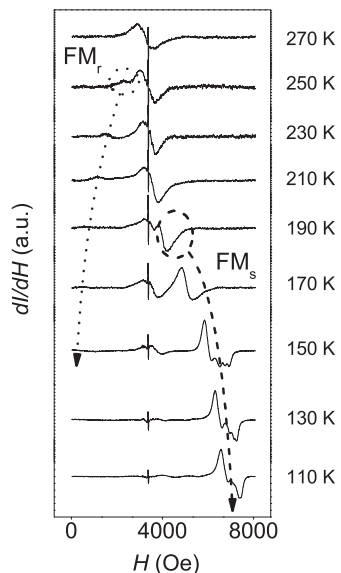


FIG. 3. Differential absorption dI/dH vs H at different temperatures measured on cooling, for \mathbf{H} applied perpendicular to the film plane. The narrow line (line 1) slightly below 4000 Oe is essentially temperature independent. The apparent variation in its height arises because the vertical scale varies between traces. Onsets for the resonances due to strained (s) and relaxed (r) FM regions are indicated.

so we identify $T_C^s \approx 190$ K. This is slightly higher than the 145 K metal-insulator transition for this sample,¹⁶ but an exact correspondence is not necessarily expected given that on cooling one expects the nucleation of FM metallic regions to precede the percolation in which most are involved.¹⁶ The PM resonance persists down to our lowest measurement temperature of 110 K, confirming the expected¹⁶ coexistence of FM and PM phases at low temperatures. The PM phase is assumed to arise within the coherently strained part of the film, given that relaxed regions should show bulk-like FM behavior.¹⁷ Thus FM_s and PM regions coexist in the coherently strained regions that form the majority of the film.

At 250 K and below, there is also a weaker ferromagnetic resonance at $H_0^{\parallel\text{FM}_r} > H_0^{\text{PM}}$ (dotted circle and arrow, Fig. 2), consistent with Eq. (3) for an out-of-the-plane magnetization with magnitude $M_0^{\text{FM}_r}$. Given that this onset temperature corresponds well to $T_C \approx 250$ K for bulk FM manganites,¹⁷ we suggest that this resonance comes from the small fraction of the film that is relaxed (satellites A and B, Fig. 1), and we use FM_r to denote this relaxed (r) FM phase, which has $T_C^r \approx 250$ K. The connectivity between the FM_r and FM_s phases is assumed to be at most rather limited, in view of their orthogonal magnetizations. The low-temperature three-phase coexistence of the PM, FM_s , and FM_r phases reveals that the FM phase seen in Ref. 16 is itself phase separated.

ESR measurements performed with \mathbf{H} applied perpendicular to the film plane (Fig. 3) provide complementary information to Fig. 2, with the FM_s and FM_r lines interchanged [see Eqs. (2) and (3)] such that $H_0^{\perp\text{FM}_s} > H_0^{\text{PM}}$ and $H_0^{\perp\text{FM}_r} < H_0^{\text{PM}}$. It is apparent here that $T_C^s \approx 190$ K (cf. Fig. 2). In addition, we find that the FM_s line comprises a superposition of a few narrower lines, suggesting that the FM_s phase is inhomogeneous, e.g., because it occupies regions of irregular shape and/or because of the influence of the other phases present. However, this interpretation is not unique as spatially nonuniform modes can be excited in spatially uniform ultrathin ferromagnetic films.²² Figure 3 also differs from Fig. 2 because the FM_r line becomes indiscernible at low temperatures, possibly due to strong line broadening.

The spectra of Fig. 2 were analyzed by fitting each line to the derivative of a single Lorentzian by using

$$\frac{dI}{dH} = \frac{2A}{\pi} \frac{d}{dH} \left[\frac{\Delta H}{4(H - H_0)^2 + \Delta H^2} \right], \quad (4)$$

where A is the area under the absorption curve, ΔH is the full width at half intensity, and H_0 is the resonance field.³⁵ We found good fits (dashed lines, Fig. 4) consistent with the presence of three phases at and below $T_C^s \approx 190$ K. Figure 5 shows the temperature dependences of the extracted linewidths ΔH^{FM_s} , ΔH^{PM} , and ΔH^{FM_r} , all of which are large in our magnetically inhomogeneous system as compared with single-phase epitaxial manganite films.³⁶ Figure 6 shows the corresponding temperature dependences of the resonance fields $H_0^{\parallel\text{FM}_s}$, H_0^{PM} , and $H_0^{\parallel\text{FM}_r}$.

On cooling, the reduction in $H_0^{\parallel\text{FM}_s}$ (Fig. 6) corresponds to an increase in $M_0^{\text{FM}_s}$ via Eq. (2), and the reduction in ΔH^{FM_s} (Fig. 5) is due to the correspondingly enhanced exchange interactions and reduced spin fluctuations. The concomitant increases in ΔH^{PM} and ΔH^{FM_r} could be due

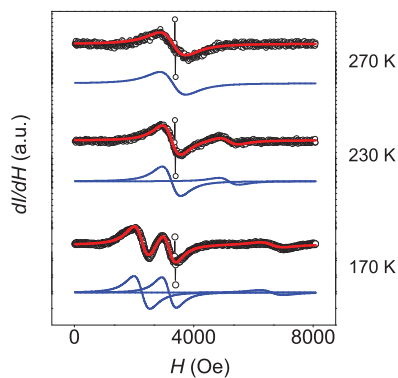


FIG. 4. (Color online) Experimental (circles) and fitted (red curves) plots of dI/dH vs H , at selected temperatures for \mathbf{H} applied parallel to the film plane. The fits were constructed by summing the derivatives of one (270 K), two (230 K), and three (170 K) Lorentzian functions (blue curves). The black lines between data points are a guide to the eye. Source data appears in Fig. 2.

to stray field from the dominant FM_s phase which changes the resonance conditions in the randomly distributed PM and FM_r phases.^{22,37} This stray field can also modify the resonance fields H_0^{PM} and $H_0^{\parallel\text{FM}_r}$ of the other phases,^{37–39} and the observed reduction of H_0^{PM} on cooling (Fig. 6) is consistent with the presence of FM regions in a thin-film geometry.²⁴

Our results may be used to estimate the temperature dependence of $M_0^{\text{FM}_s}$ and $M_0^{\text{FM}_r}$ with $g_{\text{eff}} = 2.025$ from above. It is possible that the FM_r regions, whose magnetization lies out of the film plane ($H_0^{\perp\text{FM}_r} < H_0^{\text{PM}}$), could correspond to the conducting pathways that run perpendicular to the film plane in this sample.¹⁶ If these FM_r regions were infinitely thin cylinders, then the values of $M_0^{\text{FM}_r}$ at different temperatures, deduced^{22,30} from $H_0^{\parallel\text{FM}_r}$ and $H_0^{\perp\text{FM}_r}$, agree with neither each other nor $M_0^{\text{FM}_r}(T \rightarrow 0) \sim 622 \text{ emu cm}^{-3}$ for unstrained bulk FM manganites.¹⁷ These discrepancies reach up to 30% but may be reconciled by assuming that the FM_r phase lies in ellipsoids with an aspect ratio of 0.24 such that the demagnetizing factor is 8.54 in CGS units (0.68 in SI units).²² This suggests that the FM_r phase occurs in regions that are intermediate between disks and rods, with the changes in $H_0^{\parallel\text{FM}_r}$ (Figs. 2 and 6) yielding the temperature dependence of $M_0^{\text{FM}_r}$ (triangles, Fig. 7).

For the FM_s phase whose magnetization lies in plane ($H_0^{\perp\text{FM}_s} > H_0^{\text{PM}}$), we interpret only the ESR data with \mathbf{H}

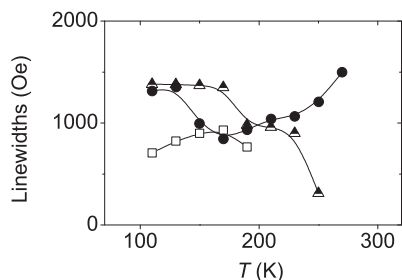


FIG. 5. The temperature dependence of linewidths ΔH^{FM_s} (squares), ΔH^{PM} (circles), and ΔH^{FM_r} (triangles) for \mathbf{H} applied parallel to the film plane. Source data appears in Fig. 2.

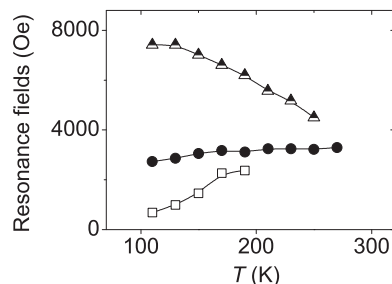


FIG. 6. The temperature dependence of resonance fields $H_0^{\parallel\text{FM}_s}$ (squares), H_0^{PM} (circles), and $H_0^{\parallel\text{FM}_r}$ (triangles) for \mathbf{H} applied parallel to the film plane. Source data appears in Fig. 2.

applied perpendicular to the film plane (Fig. 3) in order to avoid the influence of in-plane anisotropy. Assuming a demagnetizing factor of 4π yields $M_0^{\text{FM}_s} \sim 300 \text{ emu cm}^{-3}$ at low temperatures, which is lower than $M_0^{\text{FM}_r}$ due to strain, and consistent with bulk magnetometry.^{16,18} The changes in $H_0^{\perp\text{FM}_s}$ (Fig. 3) with temperature then yield the temperature dependences of $M_0^{\text{FM}_s}$ (squares, Fig. 7).

The temperature dependences of $M_0^{\text{FM}_r}$ and $M_0^{\text{FM}_s}$ may also be calculated in a mean-field approach using the Brillouin function,

$$\frac{M_0^{\text{FM}_{r,s}}(T)}{M_0^{\text{FM}_{r,s}}(T \rightarrow 0)} = B_J(X) = \frac{2J+1}{2J} \coth \left[\frac{2J+1}{2J} X \right] - \frac{1}{2J} \coth \left[\frac{1}{2J} X \right], \quad (5)$$

where $X = \frac{3J}{J+1} \frac{T_C}{T} \frac{M_0^{\text{FM}_{r,s}}(T)}{M_0^{\text{FM}_{r,s}}(T \rightarrow 0)}$ and J is the total angular momentum.²² For the doped manganites, the orbital contribution to the total angular momentum is negligible and J is given by the spin quantum number S .⁴⁰ Assuming Mn oxidation states of 3+ and 4+ with spin quantum numbers $S = 2$ and $3/2$, respectively,⁴⁰ we have $J = 0.4 \times 3/2 + (1-0.4) \times 2 = 1.8$ for $\text{La}_{0.6}\text{Ca}_{0.4}\text{MnO}_3$. Using the Curie temperatures and low-temperature saturation magnetizations from earlier, we find that the magnetization vs temperature plots for the FM_r (solid curve, Fig. 7) and FM_s (dashed curve, Fig. 7) phases agree well with the data that we extracted from resonance spectra using the Kittel equations for the distributed phases.

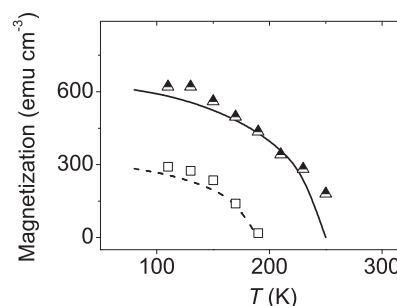


FIG. 7. Magnetizations of the ferromagnetic phases FM_r (triangles) and FM_s (squares) as functions of temperature, determined from the ESR spectra of Figs. 2 and 3 respectively. Values calculated using the Brillouin relation for FM_r (solid curve) and FM_s (dashed curve) phases are also shown.

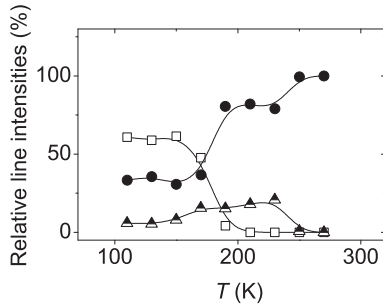


FIG. 8. Relative intensities of the FM_s (squares), PM (circles), and FM_r (triangles) resonance lines as functions of temperature. As explained in the text, these intensities are not quantitatively equal to phase fractions.

Figure 8 shows the temperature dependences of the relative intensities of the resonance peaks for the FM_s , PM, and FM_r phases, as determined at each temperature from $A_{\text{rel}}^i = A^i / \sum_{i=1}^N A^i$, where A^i is the area under the i th Lorentzian $I(H)$. These relative intensities cannot be directly interpreted as phase fractions, because the intensity per unit volume for each phase displays a potentially different temperature dependence.^{22,28,29} This explains why the low-temperature intensities in Fig. 8 are inconsistent with the $\sim 42\%$ FM volume fraction of the sample at 48 K, as determined by bulk magnetometry.¹⁶ Qualitatively, Fig. 8 shows that on cooling the FM_r phase initially grows at the expense of the PM phase, and that below T_C^s the FM_s phase coexists primarily with the PM phase.

The complexity we observe in strained manganite films is reminiscent of previous observations in which the magnetic properties of FM manganites are modified in mesoscale regions by anisotropic strain from structural defects such as twin boundaries, grain boundaries, microcracks, and dislocations.^{12,41–44} Here, coherent film strain prevents some PM regions of our film becoming FM_r ¹⁶ and modifies the dominant FM_s phase. Relaxed regions contain the minority FM_r phase, but we cannot distinguish the magnetic properties of satellite A with respect to satellite B.

Our speculation that the minority FM_r phase lies in those parts of the three-dimensional FM pathways that run perpendicular to the film plane¹⁶ is reasonable as these have an appropriately small volume fraction which may correspond to the small volume fraction of relaxed film seen by XRD. Strain release could arise at the small number of misfit dislocations

expected for a substrate-film lattice-parameter mismatch of just $\sim 0.4\%$, cf. the reduced suppression of T_C at grain boundaries in strained FM manganite films.¹² The out-of-plane magnetization in the FM_r phase is consistent with previous observations of mesoscopic magnetism in films,^{41,45} and can be reconciled with vibrating-sample magnetometer (VSM) data for this sample, where only an in-plane moment was detected,¹⁶ by assuming that the small volume fraction of the FM_r phase cannot be resolved above the strong PM signal of the NdGaO_3 substrate.

IV. SUMMARY

We have studied exactly the same epitaxial thin film of $\text{La}_{0.6}\text{Ca}_{0.4}\text{MnO}_3$ that at low temperature was found to show metallic FM regions and pathways within a PM matrix.¹⁶ XRD reveals that most of the film is coherently strained, with a small fraction relaxed. ESR reveals that the FM phase is itself phase separated into FM_s and FM_r phases. The FM_s phase is considered strained because it has a low $T_C^s \approx 190$ K and a low $M_0^{\text{FM}_s} \sim 300$ emu cm^{-3} as compared with the bulk.¹⁷ This FM_s phase occupies a large fraction of the sample that we identify to lie within the coherently strained regions seen by XRD. The PM phase coexists with the FM_s phase in these coherently strained regions, as low-temperature PM phases are only found in $\text{La}_{0.6}\text{Ca}_{0.4}\text{MnO}_3$ due to strain.^{16,18} The FM_r phase is considered relaxed because its Curie temperature $T_C^r \approx 250$ K corresponds well to the bulk value for FM phases of manganites.¹⁷ It occupies a small fraction of the sample consistent with the small fraction of relaxed film seen in XRD. The low-temperature coexistence in our film of the FM_s , FM_r , and PM phases demonstrates that manganites are prone to contain small phase fractions that cannot be detected in many standard types of macroscopic or even microscopic measurement. By reducing film thickness or nanopatterning, it may be possible to tune and exploit such minority phases in devices.

ACKNOWLEDGMENTS

The work was supported by the Joint Project of the National Academy of Sciences of Ukraine and Russian Foundation for Basic Research No. 231-11, the EU FP6 STRP CoMePhS and UK EPSRC Grant No. EP/E0026206. X.M. acknowledges support from Herchel Smith Fund. A.I.T. acknowledges support from Peterhouse, University of Cambridge, U.K.

¹R. Helmolt, J. Wecker, K. Samwer, L. Haupt, and K. Bärner, *J. Appl. Phys.* **76**, 6925 (1994).

²S. Jin, T. H. Tiefel, M. McCormack, R. A. Fastnacht, and R. Ramesh, *Science* **264**, 413 (1994).

³C. Zener, *Phys. Rev.* **82**, 403 (1951).

⁴J. C. Loudon, S. Cox, A. J. Williams, J. P. Attfield, P. B. Littlewood, P. A. Midgley, and N. D. Mathur, *Phys. Rev. Lett.* **94**, 097202 (2005).

⁵E. Dagotto, T. Hotta, and A. Moreo, *Phys. Rep.* **344**, 1 (2001).

⁶A. Tovstolytkin, A. Pogorily, A. Vovk, D. Podyalovskii, I. Lezhnenko, and A. Matviyenko, *J. Magn. Magn. Mater.* **272–276**, 1839 (2004).

⁷J. C. Loudon, N. D. Mathur, and P. A. Midgley, *Nature (London)* **420**, 797 (2002).

⁸N. Mathur and P. Littlewood, *Phys. Today* **56**, 62 (2003).

⁹M. Uehara and S.-W. Cheong, *Europhys. Lett.* **52**, 674 (2000).

- ¹⁰V. G. Prokhorov, V. A. Komashko, G. G. Kaminsky, V. L. Svetchnikov, H. W. Zandbergen, Y. P. Lee, J. S. Park, and K. W. Kim, *Low. Temp. Phys.* **29**, 117 (2003).
- ¹¹H. S. Wang, E. Wertz, Y. F. Hu, Q. Li, and D. G. Schlom, *J. Appl. Phys.* **87**, 7409 (2000).
- ¹²Y.-A. Soh, G. Aeppli, N. D. Mathur, and M. G. Blamire, *Phys. Rev. B* **63**, 020402R (2000).
- ¹³C. Israel, M. J. Calderón, and N. D. Mathur, *Mater. Today* **10**, 24 (2007).
- ¹⁴P. Levy, F. Parisi, L. Granja, E. Indelicato, and G. Polla, *Phys. Rev. Lett.* **89**, 137001 (2002).
- ¹⁵D. Casa, B. Keimer, M. v. Zimmermann, J. P. Hill, H. U. Habermeier, and F. S. Razavi, *Phys. Rev. B* **64**, 100404 (2001).
- ¹⁶C. Israel, L. Granja, T. M. Chuang, L. E. Hueso, D. Sánchez, J. L. Prieto, P. Levy, A. de Lozanne, and N. D. Mathur, *Phys. Rev. B* **78**, 054409 (2008).
- ¹⁷H. Y. Hwang and S.-W. Cheong, in *Colossal Magnetoresistive Oxides*, edited by Y. Tokura (Gordon and Breach, Amsterdam, 2000).
- ¹⁸D. Sánchez, L. E. Hueso, L. Granja, P. Levy, and N. D. Mathur, *Appl. Phys. Lett.* **89**, 142509 (2006).
- ¹⁹A. O. Badrutdinov, E. M. Zarubezhnova, Yu. I. Talanov *et al.*, *JETP* **105**, 79 (2007).
- ²⁰E. Winkler, M. T. Causa, C. A. Ramos, and E. De Biasi, *Physica B* **254**, 51 (2004).
- ²¹S. B. Ubizskii, L. O. Vasylechko, D. I. Savvytskii, A. O. Matkovskii, and I. M. Syvorotka, *Supercond. Sci. Technol.* **7**, 766 (1994).
- ²²A. G. Gurevich and G. A. Melkov, *Magnetization Oscillations and Waves* (CRC Press, Boca Raton, FL, 1996).
- ²³T. L. Phan, N. D. Tho, M. H. Phand, N. D. Ha, N. Chau, and S. C. Yu, *Physica B* **371**, 317 (2006).
- ²⁴A. I. Tovstolytkin, A. M. Pogorily, Yu. I. Dzhezherya *et al.*, *J. Phys. Condens. Matter.* **21**, 386003 (2009).
- ²⁵B. T. Jonker, A. T. Hanbicki, D. T. Pierce, and M. D. Stiles, *J. Magn. Mater.* **277**, 24 (2004).
- ²⁶Y. Liu, S. L. Wan, and X. G. Li, *J. Phys. Condens. Matter.* **19**, 196213 (2007).
- ²⁷F. Rivadulla, L. E. Hueso, C. Jardon *et al.*, *J. Magn. Magn. Mater.* **196-197**, 470 (1999).
- ²⁸A. Shengelaya, G.-M. Zhao, H. Keller, K. A. Muller, and B. I. Kochelaev, *Phys. Rev. B* **61**, 5888 (2000).
- ²⁹S. B. Oseroff, N. O. Moreno, P. G. Pagliuso *et al.*, *J. Appl. Phys.* **87**, 5810 (2000).
- ³⁰C. Kittel, *Phys. Rev.* **73**, 155 (1948).
- ³¹P. F. Fewster, *X-ray Scattering from Semiconductors* (Imperial College Press, London, 2003).
- ³²A. I. Tovstolytkin, A. N. Pogorily, I. V. Lezhnenko *et al.*, *Phys. Solid State* **45**, 1857 (2003).
- ³³F. Luis, M. D. Kuz'min, F. Bartolome, V. M. Orera, J. Bartolome, M. Artigas, and J. Rubin, *Phys. Rev. B* **58**, 798 (1998).
- ³⁴M. D. Glinchuk, I. P. Bykov, S. M. Kornienko *et al.*, *J. Mater. Chem.* **10**, 941 (2000).
- ³⁵V. A. Ivanshin, J. Deisenhofer, H.-A. Krug von Nidda, A. Loidl, A. A. Mukhin, A. M. Balbashov, and M. V. Eremin, *Phys. Rev. B* **61**, 6213 (2000).
- ³⁶R. Bah, D. Bitok, R. R. Rakhimov *et al.*, *J. Appl. Phys.* **99**, 08Q312 (2006).
- ³⁷Yu. I. Dzhezherya and A. I. Tovstolytkin, *J. Phys. Condens. Matter* **19**, 246212 (2007).
- ³⁸A. I. Tovstolytkin, A. M. Pogorily, and D. I. Podyalovskii, *Low Temp. Phys.* **35**, 130 (2009).
- ³⁹K. W. Joh, C. H. Lee, C. E. Lee, N. H. Hur, and H.-C. Ri, *J. Phys. Condens. Matter* **15**, 4161 (2003).
- ⁴⁰V. S. Amaral, J. P. Araujo, Yu. G. Pogorelov *et al.*, *J. Appl. Phys.* **83**, 7154 (1998).
- ⁴¹V. K. Vlasko-Vlasov, Y. K. Lin, D. J. Miller, U. Welp, G. W. Crabtree, and V. I. Nikitenko, *Phys. Rev. Lett.* **84**, 2239 (2000).
- ⁴²L. S. Uspenskaya, T. Nurgaliev, and T. Miteva, *J. Phys. D* **42**, 185006 (2009).
- ⁴³T. Z. Ward, J. D. Budai, Z. Gai *et al.*, *Nat. Phys.* **5**, 885 (2009).
- ⁴⁴A. Biswas, M. Rajeswari, R. C. Srivastava, Y. H. Li, T. Venkatesan, R. L. Greene, and A. J. Millis, *Phys. Rev. B* **61**, 9665 (2000).
- ⁴⁵F. Laviano, L. Gozzelino, and E. Mezzetti, *Appl. Phys. Lett.* **86**, 152501 (2005).